

## Longitudinal spin fluctuations of coupled integer-spin chains: Haldane triplet dynamics in the ordered phase of CsNiCl<sub>3</sub>

M. Enderle

*Technische Physik, Geb. 38, Universität des Saarlandes, 66123 Saarbrücken, Germany*

Z. Tun and W. J. L. Buyers

*Neutron Program for Materials Research, National Research Council Canada, Chalk River, ON, Canada K0J 1J0*

M. Steiner

*Hahn-Meitner Institut, NE, Glienickestrasse 100, 14109 Berlin, Germany*

(Received 17 December 1997; revised manuscript received 4 June 1998)

By means of high-resolution polarized neutron scattering from the spin-1 chain compound CsNiCl<sub>3</sub>, we have observed at least one additional mode of spin fluctuations, not contained in spin-wave theory, in the three-dimensional antiferromagnetically ordered phase of the material. The number of observed modes, their polarization, frequency, magnetic field dependence, and intensity show that, in contrast to the doublet-spin dynamics of conventional antiferromagnets, the Ni<sup>2+</sup> spins of CsNiCl<sub>3</sub> manifest triplet fluctuations where one component is parallel to the ordered moment. The results confirm that the Ginsburg-Landau model of Affleck and Wellman gives a realistic description of the dynamics of an ordered array of coupled integer-spin chains exhibiting the Haldane gap. The longitudinal fluctuations exist because the system lies not too far from a quantum critical point. [S0163-1829(98)00437-8]

### INTRODUCTION

In 1983 Haldane<sup>1</sup> predicted that the ground states and low-lying excitations of integer- and half-integer-spin Heisenberg antiferromagnetic (AFM) chains are different. For an *integer*-spin chain,<sup>1</sup> the ground state is a unique many-body singlet, separated by an energy gap of the order  $2JS^2 \exp(-\pi S)$  from the band of the lowest-energy excitations, where  $J$  is the coupling between spins. For *half-integer* spins<sup>1</sup> the AFM chain has low-lying excitations that extend to zero energy. The prediction of a finite energy gap for isotropic integer-spin chains at first caused considerable controversy, since both the extreme quantum  $S=1/2$  chain and the classical  $S \rightarrow \infty$  chain are known to have gapless excitations. However, subsequent numerical calculations<sup>2,3</sup> and the solution for the exactly solvable Affleck-Kennedy-Lieb-Tasaki (AKLT) model<sup>2,4</sup> have substantiated Haldane's prediction. More recent work has shown that the appearance of the Haldane gap corresponds to the breaking of a hidden symmetry of an integer-spin chain.<sup>5</sup>

Since the Haldane ground state is stable about the Heisenberg point with respect to various finite perturbations, it can be observed in real crystals containing arrays of weakly coupled AFM spin chains over quite an appreciable range of single-ion anisotropy  $D$ , provided the interchain exchange  $J'$  is reasonably small. The first material in which evidence for the Haldane gap was found<sup>6</sup> is CsNiCl<sub>3</sub>. Its Hamiltonian is

$$H = 2J \sum_i^{\text{chain}} \mathbf{S}_i \cdot \mathbf{S}_{i+1} + 2J' \sum_{\langle i,j \rangle}^{\text{plane}} \mathbf{S}_i \cdot \mathbf{S}_j + D \sum_i (\mathbf{S}_i^z)^2, \quad (1)$$

where  $D$  is the Ising-like (i.e., negative) single-ion anisotropy. The interaction between spins is almost perfectly isotropic, for the magnitude of  $D/h$  is very small, only  $-1$

GHz, as determined from the spin-flop field. The magnitudes of  $J/h$  and  $J'/h$  are 345 and 5.4 GHz, respectively.<sup>7-9</sup> Because of the small but significant interchain exchange, three-dimensional (3D) long-range order develops below 4.4 K.<sup>10</sup>

Some other systems displaying a Haldane gap are NENP, (Ref. 11) and Y<sub>2</sub>BaNiO<sub>5</sub> (Ref. 12). In these materials no long-range magnetic order has been found down to lowest temperatures. Despite its long-range order at low temperatures, in the paramagnetic phase CsNiCl<sub>3</sub> displays the characteristic behavior of a Haldane system.

(1) An energy gap over the whole Brillouin zone has been observed by neutron scattering. It is now unanimously accepted that this gap is not a trivial product of anisotropy.<sup>6,7,13</sup>

(2) The observed gap excitation is a triplet as shown unambiguously by polarized neutron experiments.<sup>13,14</sup>

(3) The spin correlations near the 1D AFM zone center,  $Q=\pi$ , in the paramagnetic phase have a length that extrapolates as  $T \rightarrow 0$  to a finite value of  $\xi=5.3$  steps along the spin chain.<sup>15</sup>

(4) The magnon dispersion along the chain axis shows periodicity  $2\pi$ , which indicates that the symmetry remains unbroken with respect to translation along the chain by one unit. Between  $Q=\pi$  and  $2\pi$ , the line width of the excitations broadens at momenta greater than  $3\pi/2$ , where the lower bound of the two-magnon continuum is expected to cross and lie below the one-magnon dispersion.<sup>14,16</sup>

(5) The excitations at the one-dimensional AFM zone center (001), although not fully resolved in unpolarized measurements, display a large field dependence<sup>17</sup> as expected for a Haldane system.<sup>18</sup>

The above results indicate that CsNiCl<sub>3</sub> in its paramagnetic phase is a quantum-disordered system located within the Haldane phase at finite temperature, but with nonzero

values of  $J'$  and  $D$ . A critical value of  $J'/J$ , estimated<sup>9,19</sup> as  $(\Delta/J)^2/48$ , is required to create the Néel phase. Since the gap  $\Delta$  renormalizes upward with temperature,<sup>9,20,21</sup> the Néel phase destabilizes rapidly with temperature. Moreover, the ordering in the Néel phase, where only half the full moment condenses, is weak as a result of the quantum fluctuations. Bearing in mind that the Néel temperature is much smaller than the energy of the gap ( $kT_N/\Delta \sim 1/3$ ), the system is seen to be close to a quantum critical point and, therefore, corresponds to the  $N=3$ ,  $d=3$  phase diagram of Sachdev.<sup>22</sup> This quantum critical point separates the singlet Haldane phase, with subcritical  $J'/J$ , from the Néel phase, whose ordered moment increases with distance from the critical point. As pointed out by Affleck and Wellman,<sup>18</sup> the longitudinal fluctuations should then be long lived and observable as peaks in the neutron scattering, at least in a bipartite lattice. In a noncollinear magnetic structure such as  $\text{CsNiCl}_3$ , the longitudinal mode interacts with the transverse modes and gains an additional mechanism for damping. In this paper we will show that the system is close enough to the quantum critical point that the extra modes arising from the mixing of longitudinal, or amplitude, and transverse fluctuations are still strong and observable, despite this interaction. Thus the characteristic Haldane triplet dynamics persist when the array of spin-1 chains enters the 3D long-range-ordered state.

We note that the behavior of the coupled  $S=1$  chains in  $\text{CsNiCl}_3$  is qualitatively similar to that of the  $S=1/2$  spin ladders, as pointed out by Normand and Rice<sup>23</sup> for  $\text{LaCuO}_{2.5}$ . The strong coupling of the two  $S=1/2$  moments essentially gives rise to a singlet-triplet (or  $S_{\text{eff}}=1$ ) structure for the lowest states of each ladder, similar to the Haldane  $S=1$  chain. Again, a critical value of interladder to intraladder coupling is required to reach the quantum critical point, which separates the spin-liquid state from the magnetically ordered state<sup>23,24</sup> and near which longitudinal fluctuations are expected.

When  $\text{CsNiCl}_3$  undergoes its magnetic transition below  $T_N=4.4$  K, the spins are antiferromagnetically ordered along each chain. The  $\text{Ni}^{2+}$  moments on adjacent chains lie in the crystallographic  $a$ - $c$  plane (denoted as the  $xz$  plane) and form a noncollinear structure where the spin directions of neighboring AFM chains are rotated by  $\sim 120^\circ$ . The ordering is described by the wave vector  $\mathbf{q}_0=(1/3,1/3,1)$ . Several experiments have shown features in the magnetic spectrum which could not be accounted for by linear spin-wave theory. As shown by Affleck and Wellman,<sup>18</sup> spin-wave theory does not apply to a 3D ordered array of Haldane chains. For an array of spin-1 atoms, the linear theory predicts incorrect frequencies and gives too few spin-wave modes.

In the Affleck-Wellman (AW) theory,<sup>18</sup> a Lagrangian is derived from the field theory for integer-spin chains: The excitations of a single chain are described by a triplet of bosons, whose minimum energy is equal to the Haldane gap energy  $\Delta$  and whose velocity is proportional to  $J$ . They are coupled together by the interchain interaction  $J'$ . The triplet nature of the Haldane gap is obtained by releasing the constraint on the magnitude of the staggered spin density along the chain. This leads to increased degrees of freedom and to new modes of magnetic excitations in the 3D ordered phase. The new modes arise from the longitudinal fluctuations of

the staggered spin density and thus are fluctuations within the plane, in which the ordered moment lies. Because of the  $120^\circ$  spin structure of  $\text{CsNiCl}_3$ , the longitudinal modes interact with those spin rotations on adjacent chains which fluctuate in the spin plane, i.e., the  $xz$  plane. The interaction of these modes gives rise to an  $xz$  spin dispersion with four doubly degenerate branches of finite intensity for a general wave vector at zero magnetic field. Their structure factor and field dependence differ greatly from those of the  $xz$  spin rotation modes of linear spin-wave theory. By contrast, the  $y$  excitations, which remain as noninteracting rotary modes perpendicular to the ordered moment, follow the dispersion of spin-wave theory. The mixing of longitudinal and transverse  $xz$  modes means that the polarization of a mode does not by itself indicate that there are longitudinal fluctuations; it is the presence of extra modes of  $xz$  symmetry, with particular dispersion and field dependence, that is required as proof.

This prediction of additional ‘‘in-plane’’ modes distinguishes the AW model from other contemporary theories which attempt to save spin-wave theory: the two-magnon spin-wave theory by Ohyama and Shiba<sup>25</sup> and the modified spin-wave theory for triangular lattices by Plumer and Caillé.<sup>26</sup> In the Ohyama-Shiba calculation additional peak-like features are obtained in  $S(\mathbf{Q},\omega)$  by taking into account the coupling of one- and two-magnon states. These features are strongest at (001) and seem to explain part of the experimental data available in 1993. However, Enderle *et al.*<sup>27</sup> have pointed out that the calculated linewidth of the two-magnon peak at  $H=0$  ( $\sim 0.2$  THz) is twice as large as the linewidth in unpolarized experiments. Moreover, Ohyama and Shiba predict a lower  $xz$  mode at (001) which should be very sharp and intense, and easily observable in polarized and unpolarized experiments. This mode has not been seen in either type of experiment, including a recent search in a high-sensitivity unpolarized experiment. In the calculation of Plumer and Caillé,<sup>26</sup> there are no extra  $xz$  modes. Their calculated  $xz$  modes at (001) do not have the same frequency as the  $y$  mode, a feature that contradicts experiments.<sup>8</sup> Affleck and Wellman predict well-defined  $xz$  excitations at (001) with about the same frequency and intensity as the  $y$  mode, while the other  $xz$  modes have vanishing intensity at (001). This is in perfect agreement with experimental observation.

Another important difference between the three models is that the triplet excitations of the AW model are predicted to show a much larger dependence on the magnetic field than do the excitations of the spin-wave theories. In particular, the Ohyama-Shiba model predicts only slight changes of the  $xz$  peak frequency and a broadening with increasing field strength. The field dependence of the Plumer-Caillé model is expected to be similarly small. However, strong field effects at 2 K were observed<sup>8,27</sup> for the two  $xz$  excitations at (001).

In previous work on the ordered phase, only two  $xz$  modes have been resolved in polarized measurements at (001) and  $(1/3, 1/3, 1)$ .<sup>8</sup> In this paper we will show, by high-resolution polarized neutron scattering, that at least three modes of  $xz$  symmetry can be clearly observed at a general wave vector and that their frequency varies rapidly in a magnetic field. Furthermore, the field and wave-vector dependence of the modes agrees with the predictions of the AW theory. This will prove that the modes of the 3D ordered phase are bands

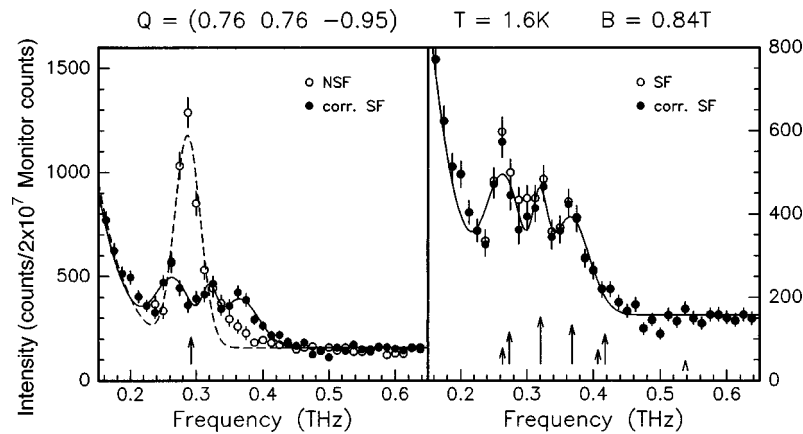


FIG. 1. Constant- $\mathbf{Q}$  scan obtained at  $\mathbf{Q}=(0.76,0.76,-0.95)$  with  $T=1.6$  K and  $B=0.84$  T.  $2 \times 10^7$  Monitor corresponds to about 39 min. NSF: non-spin flip channel corresponding to out-of-plane fluctuations, i.e.,  $y$  modes. SF: spin-flip channel corresponding to in-plane fluctuations, i.e.,  $xz$  modes. Corr. SF: the SF channel corrected for NSF feedthrough as explained in the text. The open circles, representing the uncorrected data, are obscured by the corrected data (solid circles) wherever the correction is negligible. The vertical arrows indicate magnon frequencies predicted by the Affleck-Wellman theory, with the length scaled to expected intensity. The arrow of the  $y$  mode has been scaled down by a factor of 4 with respect to the  $xz$  modes.

formed from the triplet modes of the single-chain Haldane gap excitation as modified by the interchain long-range order.

#### EXPERIMENTAL SETUP AND PROCEDURE

The inelastic scattering experiment with polarized neutrons was carried out at the NRU reactor, Chalk River. The C5 triple-axis spectrometer of the DUALSPEC facility was setup with a distance collimation of 0.67-1.2-0.85-2.0, all in degrees. Polarized neutrons were produced and analyzed by the (111) Bragg reflection of  $\text{Cu}_2\text{MnAl}$  Heusler alloy single crystals. In order to suppress fast neutron background, a liquid-nitrogen-cooled sapphire filter was installed in the reactor beam. Further background suppression was achieved by installing 1-in.-thick sapphire windows (at room temperature) before and after the analyzer. A Mezei spin flipper, required to measure spin-dependent cross sections, was installed in front of the analyzer.

The single-crystal specimen was oriented with its  $(hkl)$  plane in the scattering plane of the spectrometer. A vertical magnetic field of 0.84 T produced a single magnetic domain with the spins ordered in the horizontal plane of the spec-

trometer. Spin fluctuations within this plane are  $xz$  modes where  $\hat{x}$  and  $\hat{z}$  are vectors along the crystallographic  $a$  and  $c$  axes of the selected magnetic domain. Spin fluctuations out of the plane are  $y$  modes where  $\hat{y}$  is a vector perpendicular to  $\hat{x}$  and  $\hat{z}$  (i.e.,  $\hat{x}$ ,  $\hat{y}$ , and  $\hat{z}$  is a Cartesian system). Since the applied field and, hence, the neutron polarization were along  $\hat{y}$ , the  $xz$  modes appeared as spin-flip (SF) scattering, while the  $y$  modes gave rise to non-spin-flip (NSF) scattering. The polarized neutron experiment therefore allowed us to unambiguously distinguish the two types of orthogonal fluctuations.

Constant- $\mathbf{Q}$  scans were carried out with a fixed final neutron energy  $E_f$  of 2.5 THz. The relatively low  $E_f$  was needed to achieve high-energy resolution. However, it presented a special problem in tuning the Mezei flipper (i.e., adjusting the currents to precisely rotate neutron spins by  $\pi$ ), since no neutron filter was available at 2.5 THz to remove higher-order neutrons that would have been rotated less. This problem was overcome by tuning the flipper at magnetic Bragg reflections of  $\text{CsNiCl}_3$  which were free from higher-order contamination. We chose to tune the flipper at the magnetic Bragg reflection  $(1/3, 1/3, -1)$  since no magnetic Bragg scattering existed at  $(2/3, 2/3, -2)$ , while the nuclear reflection

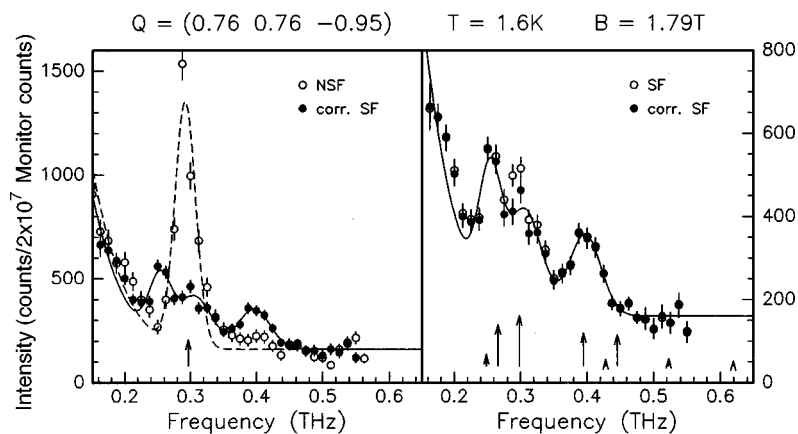


FIG. 2. Constant- $\mathbf{Q}$  scan obtained at  $\mathbf{Q}=(0.76,0.76,-0.95)$  with  $T=1.6$  K, same as for Fig. 1, but at a higher field  $B=1.79$  T.

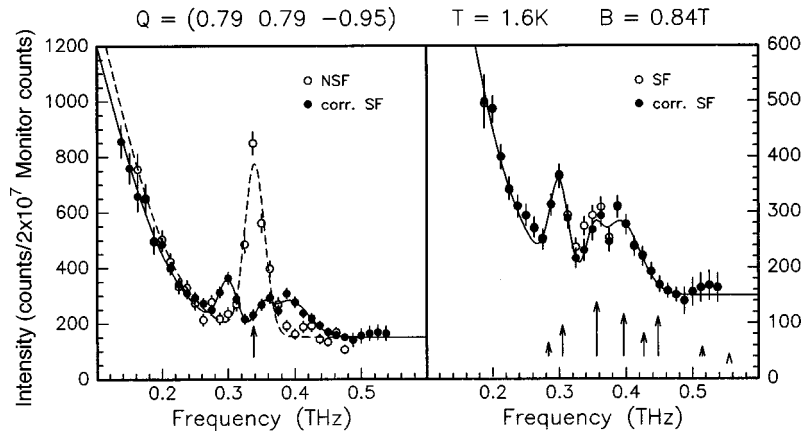


FIG. 3. Constant- $\mathbf{Q}$  scan obtained at  $\mathbf{Q}=(0.79,0.79,-0.95)$  with  $T=1.6$  K, same as for Fig. 1, at  $B=0.84$  T.

(1, 1, -3) was systematically absent. The flipper was thus tuned at each value of applied field and subsequently checked at several other magnetic Bragg reflections. The procedure typically gave a flipping ratio greater than 23 at (1/3, 1/3, -1), which was more than adequate to perform the experiment. It also allowed us to verify that the sample remained in the single-domain state during temperature and field cycles.

The wave vectors were chosen so as to match the spectrometer resolution function to the velocity of the spin excitations along the chain direction. Because of their high velocity along  $c^*$ , it was easy to achieve and fine-tune focusing by choosing wave vectors ( $hhl$ ) with  $l$  slightly different from -1, almost independent of the value of the low-velocity component  $h$ . The results are nonetheless typical of the dispersion along the basal plane direction, the direction that is most sensitive to the interchain coupling. In this highly focused configuration the measured inelastic peaks were very sharp. We considered possible spurions of several types: (1) higher-order Bragg scattering at polarizer and analyzer, and incoherent elastic scattering at the sample ( $nk_i-i-mk_f$ ), (2) higher-order Bragg scattering at the polarizer, Bragg scattering at the sample, and incoherent elastic scattering at the analyzer ( $nk_i-b-i$ ), and (3) incoherent elastic scattering at the polarizer, Bragg scattering at the sample, and higher-order Bragg scattering at the analyzer ( $i-b-nk_f$ ). The closest spurions of the type  $nk_i-i-mk_f$  would be the  $n=6, m=7$  spurion at 0.903 THz and the  $n=7, m=8$  spurion

at 0.765 THz, both outside the region of interest. The only spurions of the type  $nk_i-b-i$  or  $i-b-nk_f$  coming into question are those with  $n=4$  on nuclear Bragg peaks which would appear unpolarized. Phonons would not appear in the spin-flip channel. These tests confirm that the peaks are indeed magnetic. This was further substantiated by observing that the peak frequencies and intensities varied with magnetic field.

## RESULTS AND DISCUSSION

Constant- $\mathbf{Q}$  scans obtained at  $T=1.6$  K at several wave vectors ( $h, h, -0.95$ ) and two different magnetic field strengths (0.84 and 1.79 T) are displayed in Figs. 1–6. Figures 7 and 8 show scans at a wave vector with a slightly different  $c^*$  component  $\mathbf{Q}=(0.765, 0.765, -0.97)$ . A Gaussian fit to the incoherent elastic peak and to the peaks due to several magnetic excitations is shown. There is a single peak in the NSF channel, which corresponds to out-of-plane  $y$  fluctuations. Its extremely small width compared to the width of the incoherent elastic scattering peak attests to the finely tuned focusing achieved by selecting the  $c^*$  component of  $\mathbf{Q}$ . The high-energy tail of the inelastic peak is also a result of the focusing geometry. Three Gaussians are required to fit the finite energy peaks observed in the SF scattering channel which arise from  $xz$  fluctuations. Most of the fitted peaks correspond to a resolved spin excitation of dominant intensity, and the fitted widths of such peaks are

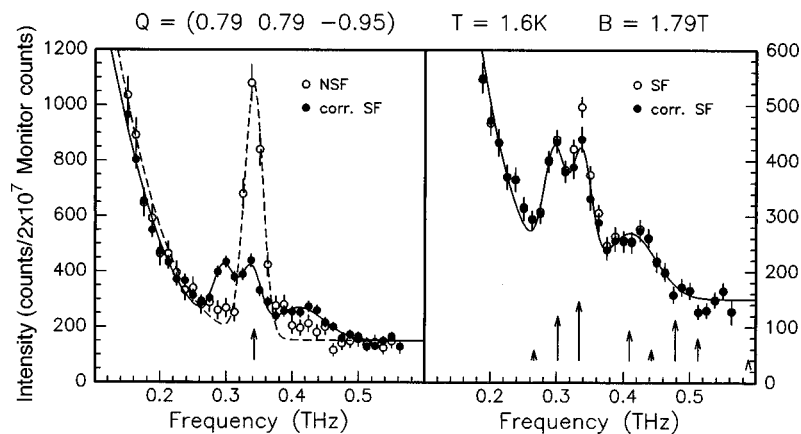


FIG. 4. Constant- $\mathbf{Q}$  scan obtained at  $\mathbf{Q}=(0.79,0.79,-0.95)$  with  $T=1.6$  K, same as for Fig. 1, at  $B=1.79$  T.

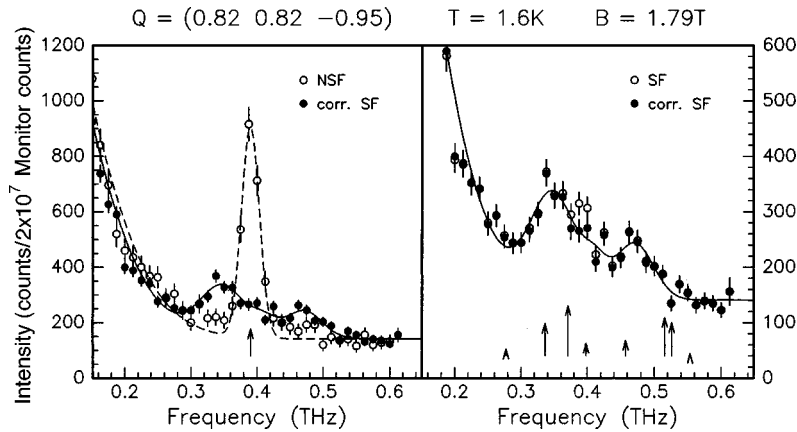


FIG. 5. Constant- $\mathbf{Q}$  scan obtained at  $\mathbf{Q}=(0.82,0.82,-0.95)$  with  $T=1.6$  K, same as for Fig. 1, at  $B=1.79$  T.

comparable to the fitted widths of the single-mode  $y$  peaks. This remains true even if a second peak of much weaker intensity lies within the resolution range. Some of the peaks, such as the highest-frequency SF peak Fig. 4, have a larger fitted width because they are composed of more than one spin excitation. The presence of such a broadened peak has been used as evidence for the existence of at least one spin excitation, which is the most conservative approach when counting the number of  $xz$  modes. Because the  $y$  peak is much stronger than the  $xz$  peaks, there is a small but significant feedthrough of the NSF intensity into the SF channel. Using the flipping ratios measured at neighboring magnetic Bragg peaks, the NSF feedthrough could be calculated and subtracted from the measured SF intensities. The intensities thus corrected are shown together with raw data on the right-hand-side panel of the figures. Note that for the wave vectors  $\mathbf{Q}=(0.76,0.76,-0.95)$  (Fig. 1) and  $\mathbf{Q}=(0.79,0.79,-0.95)$  (Fig. 3) the  $xz$  modes do not coincide with the  $y$  mode, neither in the raw data nor in the corrected data. This gives us assurance that the  $xz$  peaks are real and not caused by the strong NSF peak or correction. Moreover, at least three  $xz$  peaks are seen to exist at  $\mathbf{Q}=(0.76,0.76,-0.95)$  and  $\mathbf{Q}=(0.79,0.79,-0.95)$ , whereas spin-wave theory predicts only two  $xz$  modes strong enough to be observed (see Fig. 2 of Morra *et al.*,<sup>7</sup> which is a sufficiently good description of spin-wave theory for almost isotropic  $\text{CsNiCl}_3$ ). Thus, given that some of the peaks may represent unresolved mag-

nons, there is *at least* one extra mode in the in-plane  $xz$  fluctuations. Although the width of the three peaks is obviously different, all three are much sharper than the additional two-magnon features of Ohyama and Shiba.<sup>25</sup>

Figures 1 and 2, 3 and 4, 7 and 8 display pairs of spectra measured at the same  $\mathbf{Q}$  and temperature, but different magnetic fields  $B=0.84$  T (Figs. 1, 3, and 7) and  $B=1.79$  T (Figs. 2, 4, and 8). There is no visible shift of the  $y$ -mode frequency with the field. We still require three Gaussians for the finite-energy  $xz$  peaks at the higher field strength, but they are now found to be at different frequencies: the lowest and middle peaks shift down, while the upper mode shifts significantly up in frequency. Hence all three  $xz$  peaks respond to the field, confirming that they are real magnetic excitations. Neither the  $xz$  magnons of linear theory nor those of the two special spin-wave models<sup>25,26</sup> would show measurable frequency shifts for field changes as small as in our experiment. Moreover, these theories predict the field dependence of the  $xz$  modes to be *smaller* than that of the  $y$  mode.<sup>25,26</sup> Affleck and Wellman, on the other hand, predict a larger field dependence for the  $xz$  modes. The observation of  $xz$  magnons with *larger* field dependence than the  $y$  magnon gives strong support to the AW model.

For a detailed comparison between experiment and AW theory,<sup>18</sup> we have recalculated the expected magnon frequencies and intensities at exactly the wave vectors (i.e., with the  $c^*$  component  $=-0.95$  and  $-0.97$ , respectively) and the

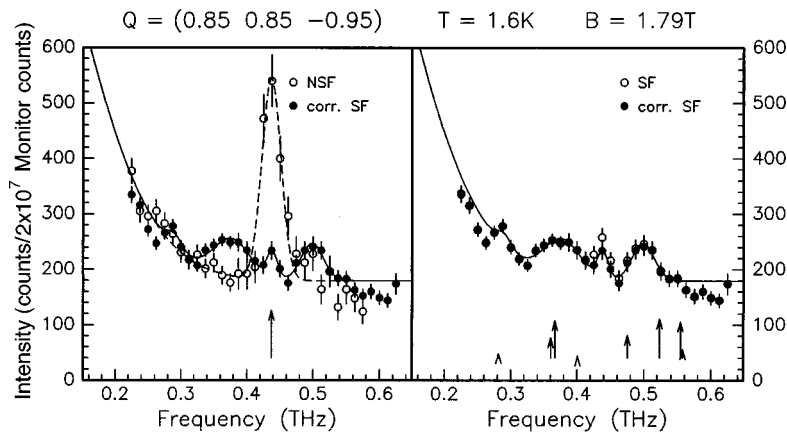


FIG. 6. Constant- $\mathbf{Q}$  scan obtained at  $\mathbf{Q}=(0.85,0.85,-0.95)$  with  $T=1.6$  K, same as for Fig. 1, at  $B=1.79$  T.

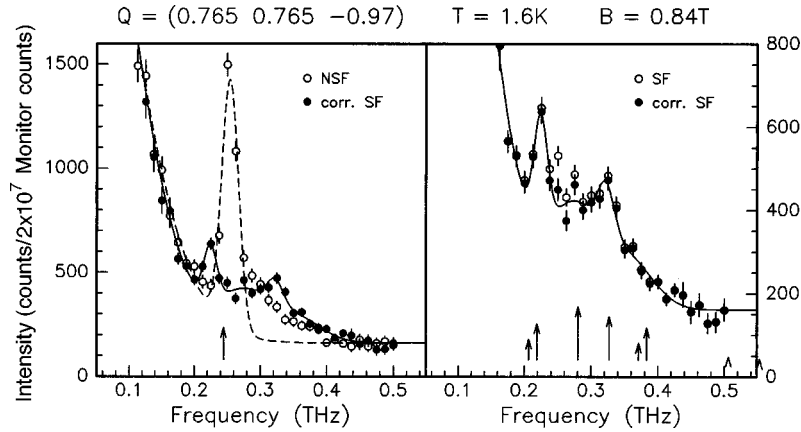


FIG. 7. Constant- $Q$  scan obtained at  $Q=(0.765,0.765,-0.97)$  with  $T=1.6$  K, same as for Fig. 1, at  $B=0.84$  T.

fields we chose for the measurements. The calculation (see the Appendix), involving diagonalizing a matrix given by Affleck and Wellman, was performed with the same parameters used previously to explain the zero-field dispersion:  $J/h=345$  GHz,  $J'/h=5.4$  GHz, and  $\Delta/h=214$  GHz, where  $\Delta$  is the Haldane excitation gap of a single chain. The moment is related to the spin by  $g_{\perp}=2.28$ , as known from susceptibility and electron-spin resonance (ESR) experiments.<sup>28</sup> The experimental and theoretical results are depicted in two ways: in Figs. 1–8 the calculated mode frequencies are shown by vertical arrows whose length is scaled to expected intensities, and the frequencies and intensities, respectively, are plotted as a function of wave vector ( $\eta, \eta, -0.95$ ) in Figs. 9 and 10. Note that, e.g.,  $\eta=0.24$  is equivalent to the experimental wave vector (0.76, 0.76,  $-0.95$ ) in Figs. 1 and 2. The circles in Fig. 9 show the positions of Gaussian peaks fitted to a scan. The eight predicted  $xz$  branches which are split from the original four by the magnetic field are numbered in order of increasing energy at the ordering vector.

It is clear that there is a very good agreement for the  $y$ -mode frequency (see Figs. 1–8 and 9). The fact that the frequency does not shift with field is expected from AW theory and, indeed, from all other theories proposed for  $\text{CsNiCl}_3$ . This is no surprise, since the longitudinal fluctuations of the staggered spin density do not mix into the  $y$  mode for zero Ising anisotropy, which is a good approximation for  $\text{CsNiCl}_3$ . At a first glance one might be surprised

that the peak intensity of the  $y$  mode above background increases by as much as  $\sim 30\%$  with the field (cf. Figs. 1 and 3 with 2 and 4, respectively). However, the integrated intensity *decreases* by about 10%, indicating that the peak intensity increase is an artifact caused by a slight change in the focusing geometry. Moreover, at the close-by wave vector  $Q=(0.765, 0.765, -0.97)$  (Figs. 7 and 8) the peak intensity of the  $y$  mode decreases with the field. Because of this sensitivity to slight changes in the focusing geometry, we do not use our data for comparison of absolute intensities between different wave vectors or magnetic fields. However, a comparison of relative intensities in the same scan remains still reasonable.

We will now compare calculated and measured  $xz$  modes. Given the possibility that some of the  $xz$  modes may not be observable due to the finite lifetime of longitudinal fluctuations,<sup>18</sup> the qualitative overall agreement for the  $xz$  modes is surprisingly good (see Fig. 9). At both field values, the wave-vector dependence of the frequencies is reproduced by the calculation. Moreover, the field dependence of the observed modes is in perfect agreement with the calculated frequencies. In the following, we discuss the spectra in detail, starting from the experimental wave vector ( $\eta, \eta, -0.95$ ) with the highest  $\eta$ . At  $\eta=0.24$ , corresponding to (0.76, 0.76,  $-0.95$ ) in the experiment (Figs. 1 and 2), we observe at both field values the three modes with the strongest calculated intensity, modes 2, 3, and 4. According to the intensity calculation, mode 6 should be observed as well. All

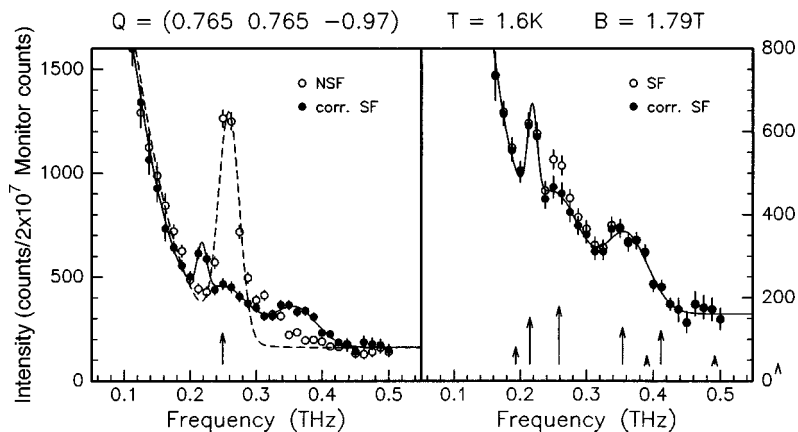


FIG. 8. Constant- $Q$  scan obtained at  $Q=(0.765,0.765,-0.97)$  with  $T=1.6$  K, same as for Fig. 1, at  $B=1.79$  T.

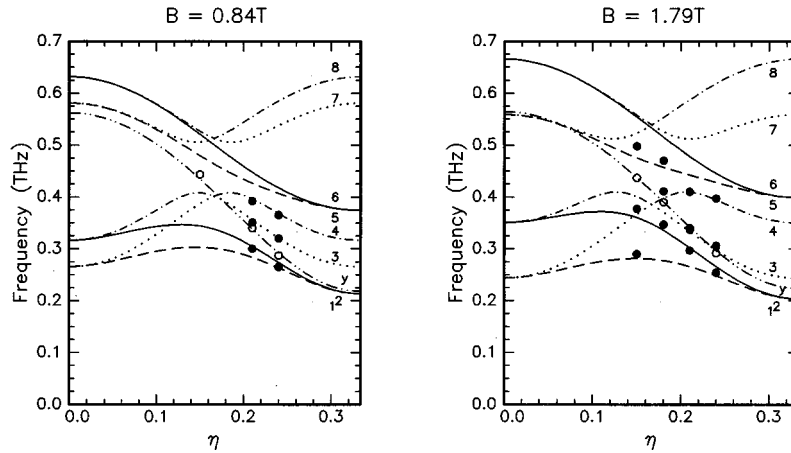


FIG. 9. Magnon branches predicted by the Affleck-Wellman theory for wave vectors  $(\eta, \eta, -0.95)$  and in an applied field  $B$ . The single  $y$  mode is labeled “ $y$ ,” while the  $xz$  modes are numbered (1–8) in ascending order of the frequencies at the ordering vector. Positions of the Gaussians fitted to constant- $Q$  data are circles, solid symbols for  $xz$  (SF) modes and open symbols for  $y$  (NSF).

other modes have much less predicted intensity, in agreement with the observation. At  $\eta=0.21$  (see Figs. 3 and 4), we observe again modes 2, 3, and 4, but not 6. The intensity of mode 6 should now be comparable to or higher than that of modes 2 and 4. Two other modes with significant predicted intensity are missing in the experiment: At 0.84 T, the calculation predicts mode 5 with an intensity comparable to that of mode 2; at 1.79 T, mode 7 gains a strength comparable to mode 4. Other modes carry too small intensity to be observed in agreement with the experiment. At  $\eta=0.18$  (Fig. 5), we have data only at 1.79 T. We still observe modes 2, 3, and 4, but now also mode 5. However, modes 6 and 7, which are predicted to be considerably stronger than modes 4 and 5, are not observed. At  $\eta=0.15$ , for  $B=1.79$  T, the observed peaks are rather broad and correspond to the unresolved excitations of modes 2 and 3, and 5, 6, and 7. There is a faint feature at the position of mode 1 which corresponds to a weak mode in the calculation. The spectra at  $\eta=0.235$  with  $c^*$  of  $-0.97$  (Figs. 7 and 8) are very similar to those at  $\eta=0.24$ , with  $c^*$  of  $-0.95$ , and confirm that our conclusions do not depend on a special choice of the small  $c^*$  component.

The above discussion can be summarized as follows: The most serious discrepancies concerning  $xz$  modes are not

observing mode 6 at any wave vector and not observing modes 5 and 7 at some wave vectors. If we now look at the longitudinal contribution to the eigenvectors (see Table I), we find a very plausible explanation: The eigenvectors of modes 5, 6, and 7 are predominantly longitudinal for all values of  $\eta$  with longitudinal components between 68% and 100%, while modes 2, 3, and 4 are predominantly transverse, their longitudinal components ranging between 0 and 32% (see Table I). Therefore a finite lifetime should be expected to detect than a sharp excitation of comparable intensity. In this sense, the direct observation of mode 5, for  $B=1.79$  T at  $\eta=0.15$  and  $\eta=0.18$ , is the cleanest model-free evidence that longitudinal modes exist in the three-dimensionally ordered phase of this, and presumably other, Haldane systems.

## CONCLUSION

Our high-resolution polarized-neutron-scattering experiment on  $\text{CsNiCl}_3$  has revealed *at least* one additional excitation branch, which is not contained in spin-wave theory. This direct observation, as well as the polarization, frequency, and magnetic field dependence of the observed excitations, is in excellent agreement with the predictions of the Affleck-

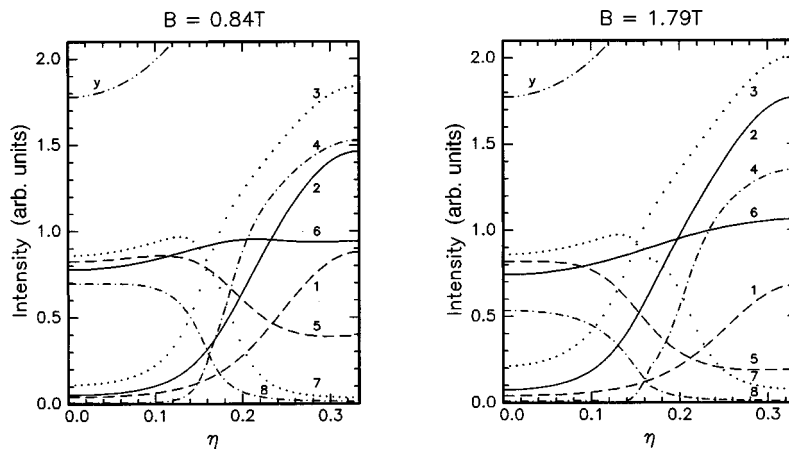


FIG. 10. Calculated intensities of the magnon branches shown in Fig. 9.

TABLE I. Contribution of the longitudinal component of the eigenvectors,  $|\tilde{\phi}_L|^2$ , for the different modes shown in Figs. 1–6, 9 and 10 (in %).

Mode	$B = 0.84$ T			$B = 1.79$ T		
	$\eta = 0.21$	0.24	0.15	0.18	0.21	0.24
1	11	6	27	22	16	11
2	0	0	2	0	2	4
3	24	30	3	19	27	32
4	10	22	31	7	1	13
5	100	98	100	97	92	88
6	85	91	68	72	76	80
7	92	80	64	87	100	93
8	73	67	92	75	68	64

Wellman model. There is even reasonable qualitative agreement of observed and calculated intensities with an indication that modes with a large contribution from longitudinal fluctuations have a finite lifetime and hence are harder to observe. Our results cannot be explained by the two-magnon

spin-wave theory<sup>25</sup> or by another modified spin-wave theory for triangular lattices.<sup>26</sup> Our experiment shows that, even in the three-dimensionally long-range-ordered antiferromagnetic phase, strong longitudinal quantum fluctuations exist parallel to the ordered moments. They are the signatures of the triplet excitations from the Haldane ground state of a single chain. Hence CsNiCl<sub>3</sub> is an example of a quasi-one-dimensional system close to the quantum critical point.

#### ACKNOWLEDGMENTS

We are grateful to AECL for provision of the neutron beam facilities, to R. L. Donabarger for technical assistance, and to I. Affleck for useful discussions. M. E. received support by the German Bundesministerium für Bildung, Wissenschaft, Forschung und Technologie (Project No. KN04SAA-06).

#### APPENDIX

The equation which has been used to determine the field-dependent  $xz$  frequencies and intensities is Eq. (4.17) in Ref. 18:

$$\begin{pmatrix} -E^2 + 4J'S\nu(3-f) + [\nu\pi(1-\zeta)]^2 & -i(2g\mu_B HE + 4\sqrt{3}J'S\nu\tilde{f}) \\ -i(2g\mu_B HE + 4\sqrt{3}J'S\nu\tilde{f}) & -E^2 + 4J'S\nu(3-f) + [\nu\pi(1-\zeta)]^2 + \Delta_L^2 + 2(g\mu_B H)^2 \end{pmatrix} \begin{pmatrix} \tilde{\phi}_1 \\ \tilde{\phi}_L \end{pmatrix} = 0,$$

where  $E$  is the frequency,  $S=1$ ,  $\nu=4JS$ ,  $\Delta_L^2=24J'S\nu-2\Delta^2$ ,  $\Delta$  is the Haldane gap of a single chain as before,  $f=2\cos(2\pi\eta)+\cos(4\pi\eta)$ ,  $\tilde{f}=2\sin(2\pi\eta)-\sin(4\pi\eta)$ , and  $\mathbf{Q}=(\eta\eta\zeta)$ .  $\tilde{\phi}_1$  and  $\tilde{\phi}_L$  are the transverse and longitudinal

component of the eigenvector with respect to the staggered spin density. The eigenvectors are normalized with  $|\tilde{\phi}_1|^2 + |\tilde{\phi}_L|^2 = 1$ .  $S(q, \omega)$  has been calculated from the eigenvectors in analogy to Eq. (2.45) in Ref. 18.

<sup>1</sup>F. D. M. Haldane, Phys. Lett. **93A**, 464 (1983); Phys. Rev. Lett. **50**, 1153 (1983).

<sup>2</sup>I. Affleck, J. Phys.: Condens. Matter **1**, 3047 (1989) (review) and references therein.

<sup>3</sup>M. Takahashi, Phys. Rev. Lett. **62**, 2313 (1989).

<sup>4</sup>I. Affleck, T. Kennedy, E. H. Lieb, and H. Tasaki, Phys. Rev. Lett. **59**, 799 (1987); Commun. Math. Phys. **115**, 477 (1988).

<sup>5</sup>G. Gómez-Santos, Phys. Rev. Lett. **63**, 790 (1989); M. den Nijs and K. Rommelse, Phys. Rev. B **40**, 4709 (1989); S. M. Girvin and D. P. Arovas, Phys. Scr. **T27**, 156 (1989); H. Tasaki, Phys. Rev. Lett. **66**, 798 (1991); Y. Hatsugai and M. Kohmoto, Phys. Rev. B **44**, 11 789 (1991); T. Kennedy and H. Tasaki, *ibid.* **45**, 304 (1992); M. Oshikawa, J. Phys.: Condens. Matter **4**, 7469 (1992).

<sup>6</sup>W. J. L. Buyers, R. M. Morra, R. L. Armstrong, M. J. Hogan, P. Gerlach, and K. Hirakawa, Phys. Rev. Lett. **56**, 371 (1986).

<sup>7</sup>R. M. Morra, W. J. L. Buyers, R. L. Armstrong, and K. Hirakawa, Phys. Rev. B **38**, 543 (1988).

<sup>8</sup>K. Kakurai, M. Steiner, R. Pynn, and J. K. Kjems, J. Phys.: Condens. Matter **3**, 715 (1991).

<sup>9</sup>I. Affleck, Phys. Rev. Lett. **62**, 474 (1989); **65**, 2477(E) (1990); **65**, 2835(E) (1990).

<sup>10</sup>R. H. Clark and W. G. Moulton, Phys. Rev. B **5**, 788 (1972); W. B. Yelon and D. E. Cox, *ibid.* **7**, 2024 (1973).

<sup>11</sup>L. P. Regnault, I. Zalizniak, J. P. Renard, and C. Vettier, Phys. Rev. B **50**, 9174 (1994) and references therein; S. Ma, C. Broholm, and D. H. Reich, Phys. Rev. Lett. **69**, 3571 (1992).

<sup>12</sup>G. Xu, J. F. DiTusa, T. Ito, K. Oka, H. Takagi, C. Broholm, and G. Aeppli, Phys. Rev. B **54**, R6827 (1996) and references therein; J. Darriet and L. P. Regnault, Solid State Commun. **86**, 409 (1993).

<sup>13</sup>M. Steiner, K. Kakurai, J. K. Kjems, D. Petitgrand, and R. Pynn, J. Appl. Phys. **61**, 3953 (1987).

<sup>14</sup>Z. Tun, W. J. L. Buyers, R. L. Armstrong, E. D. Hallman, and D. P. Arovas, J. Phys. (Paris), Colloq. **49**, Suppl. 12, C8-1431 (1988).

<sup>15</sup>K. Kakurai, Physica B **180&181**, 153 (1992).

<sup>16</sup>Z. Tun, W. J. L. Buyers, R. L. Armstrong, K. Hirakawa, and B. Briat, Phys. Rev. B **42**, 4677 (1990).

<sup>17</sup>M. Enderle, K. Kakurai, M. Steiner, and H. Weinfurter, J. Magn. Magn. Mater. **104–107**, 809 (1992).

<sup>18</sup>I. Affleck and G. F. Wellman, Phys. Rev. B **46**, 8934 (1992).

<sup>19</sup>T. Sakai and M. Takahashi, Phys. Rev. B **42**, 4537 (1990).

<sup>20</sup>W. J. L. Buyers, Z. Tun, A. Harrison, J. A. Rayne, and R. M.

- Nicklow, *Physica B* **180&181**, 222 (1992).
- <sup>21</sup>H. Köhler and R. Schilling, *J. Phys.: Condens. Matter* **4**, 7899 (1992).
- <sup>22</sup>S. Sachdev, in *Dynamical Properties of Unconventional Magnetic Systems*, Vol. 349 of *NATO Advanced Study Institute, Series E: Applied Sciences*, edited by A. Skjeltorp and D. Sherrington (Kluwer Academic, Dordrecht, 1998).
- <sup>23</sup>B. Normand and T. M. Rice, *Phys. Rev. B* **56**, 8760 (1997).
- <sup>24</sup>M. Troyer, M. E. Zhitomirsky, and K. Ueda, *Phys. Rev. B* **55**, R6117 (1997).
- <sup>25</sup>T. Ohyama and H. Shiba, *J. Phys. Soc. Jpn.* **62**, 3277 (1993); **63**, 3454 (1994).
- <sup>26</sup>M. L. Plumer and A. Caillé, *Phys. Rev. Lett.* **68**, 1042 (1992).
- <sup>27</sup>M. Enderle, K. Kakurai, K. N. Clausen, M. Steiner, T. Inami, and H. Tanaka, *Physica B* **213&214**, 158 (1995).
- <sup>28</sup>N. Achiwa, *J. Phys. Soc. Jpn.* **27**, 561 (1969).